Influence of the laser pulse steep rising front on ion acceleration

M. Matys[1,2], S. V. Bulanov[1,3], M. Kucharik[2], M. Jirka[1,2], J. Nikl[1,2],
M. Kecova[1], J. Proska[2], J. Psikal[1,2], G. Korn[1] and O. Klimo[1,2]

[1] *ELI Beamlines Centre, IoP, Czech Academy of Sciences, Dolni Brezany ,Czech Republic*

[2] *FNSPE, Czech Technical University in Prague, Prague, Czech Republic*

[3] *Kansai Photon Science Institute - QST, Kyoto, Japan*

Introduction of a steep-rising front at the beginning of the laser pulse substantially influences electron and ion dynamics in the irradiated target, including generation of high density particle bunches and mitigation of specific transverse instabilities [1, 2]. The steep rising front can be produced by the plasma shutter [3–8], a thin solid foil placed in front of the target. This approach also reduces prepulse and locally increases laser intensity [9] at the cost of losing a part of the laser pulse energy. Consequently, it results in increase of the ion energy [10, 11] and decrease of the divergence of ion beam accelerated from the target located behind the shutter [11].

In this work, we study the plasma shutter interaction with a PW-class laser (corresponding to systems like ELI Beamlines) and subsequent interaction of the transmitted laser pulse with a silver foil using 2D and 3D particle-in-cell (PIC) simulations (code EPOCH [12]) and their combination with 2D hydrodynamic simulations (code PALE [13]) simulating the influence of a sub-ns prepulse on the double-shutter configuration.

The simulations consist of a fully ionized silicon nitride plasma shutter of electron density $n_e = 835\ n_c$ and thickness $d = 20$ nm, a partially ionized silver target (charge number $Z = 40$ and mass number $A = 108$) of $n_e = 2100\ n_c$ and $d = 20$ nm and a linearly polarized laser pulse with wavelength $\lambda = 1\ \mu$m (thus the critical density corresponds to $n_c \approx 1.115 \times 10^{21}$ cm^{-3}). The laser pulse has a Gaussian spatial profile with the full width at half maximum (FWHM) equal to 3 λ. The temporal profile has a

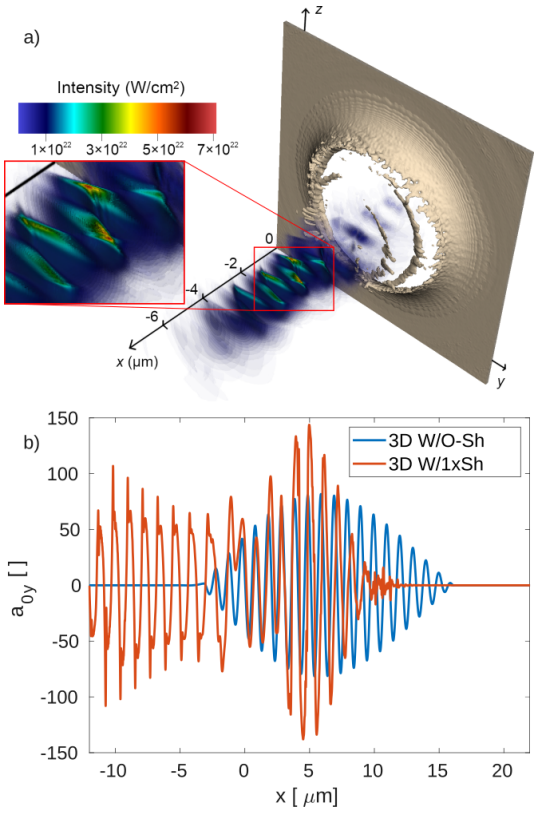

Figure 1: *Plasma shutter: (a) 3D visualization with highlighted 2D slice of intensity profile, source [9]. (b) Central 1D profile of dimensionless amplitude of the electric field in the y-direction (a_{0y}) at later time, source [10].*

$\sin^2(t)$ shape in intensity and beam duration is 64 fs. The pulse roughly corresponds to a 30 fs long 1 PW laser pulse with a Gaussian shape. The peak intensity is $I_{\max} = 1 \times 10^{22}$ W/cm^2, thus yielding dimensionless amplitude $a_0 = eE_0/m_e\omega c \approx 0.85\sqrt{I\,[10^{18}\mathrm{W/cm^2}]\,\lambda^2\,[\mu\mathrm{m}]} \approx 85$. Here, E_0 is the electric field amplitude, ε_0 is permittivity of vacuum, ω is laser angular frequency, m_e and e are electron mass and charge, respectively, and c is speed of light in vacuum.

The effects of the transmittion of the laser pulse through the plasma shutter are shown in Fig. 1. The relativistic plasma aperture [14] is generated, laser pulse is diffracted and its constructive interference with generated high harmonics leads to the local intensity increase by the factor of 7 in our 3D simulation [9]. Fig. 1-b shows the central 1D slice of electric field at later time when the 1D profile stabilized. The transmitted laser pulse acquires the steep-rising front and is about 5 periods shorter [10, 11].

In the next step we investigated the effect of these pulse modifications on ion acceleration from the silver target [11], comparing the cases without (W/O-Sh) and with the shutter (W/1xSh). When the plasma shutter is included in our simulations a beam-like structure in ion density (green) appears around the laser axis as can be seen in Fig. 2, resulting in reduction of the divergence [11] from 35° to 5° for x-z and from 28.5° to 18.5° for x-y planes compared to the simulation without the shutter. The steep rising front (and increased intensity) generated by the plasma shutter also results in increase of maximal silver ion energy by 35 % (from 115 MeV/A to 155 MeV/A) as can be seen in the inset of Fig. 2.

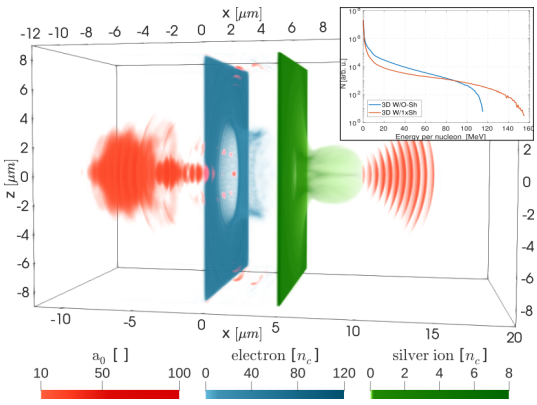

Figure 2: *Visualization of our 3D simulation of plasma shutter (blue), main target (green) and laser pulse (red). Inset contains silver ion energy spectra at the end of simulation [11].*

The changes can be explained by different electron (and consequently ion) dynamics when the steep front is introduced. Fig. 3 shows the electron density of the silver target in simulations with the plasma shutter (Fig. 3-a) and without it (Fig. 3-b) during the interaction with the laser pulse [11]. In the simulation with the steep front (Fig. 3-a) a high density electron bunches are generated around the laser axis ($z = 0$) in the x-z plane (for discussion about x-y and y-z planes and the bunches coupling with the generated magnetic field in the y-direction exceeding 4 gigagauss see Ref. [11]). On the contrary, in Fig. 3-b the structures in electron density are pre-expanded by the relatively long low-intensity part of the time profile of the incoming laser pulse (blue line in Fig. 1-b) before the interaction with the high-intensity part.

The differences in the distribution of electron density then manifests itself also in the corresponding ion distributions via the generated electric field in the z-direction as discussed in Ref. [11].

In order to take prepulse into account, we combined the 2D particle-in-cell simulations with 2D hydrodynamic ones assuming the double-shutter scenario. The first plasma shutter was pre-expanded by a prepulse with intensity $I = 1 \times 10^{12}$ W/cm^2 and duration of 125 ps using the hydrodynamic simulation (treatment of ns prepulses by other techniques like using the plasma mirrors [15] is assumed). The final 2D density profile was subsequently imported into the initial condition of 2D PIC simulation. Therefore, its configuration is the pre-expanded shutter, the non-expanded shutter and the silver target with spacing of 5 μm between each of them (see Fig. 9-a in Ref. [11]). The comparison of the silver ion energy spectra of this case (reffered to as W/2xSh) to 2D counterparts of the cases without (W/O-Sh) and with non-expanded single shutter (W/1xSh) is shown in Fig. 4. The energy spectra of the cases with single and double shutters are very similar for ions with energy up to 160 MeV/A.

The addition of the pre-expanded shutter affected only the most energetic ions. A significant increase of ion energy compared to the case without shutter is visible also for the double shutter case.

Note that the energies of the W/O-Sh simulation is overestimated as no prepulse was assumed in it. The corresponding simulation with silver target pre-expanded by the same 125 ps long prepulse is represented by the purple solid line (W/O-Sh-PP). Com-

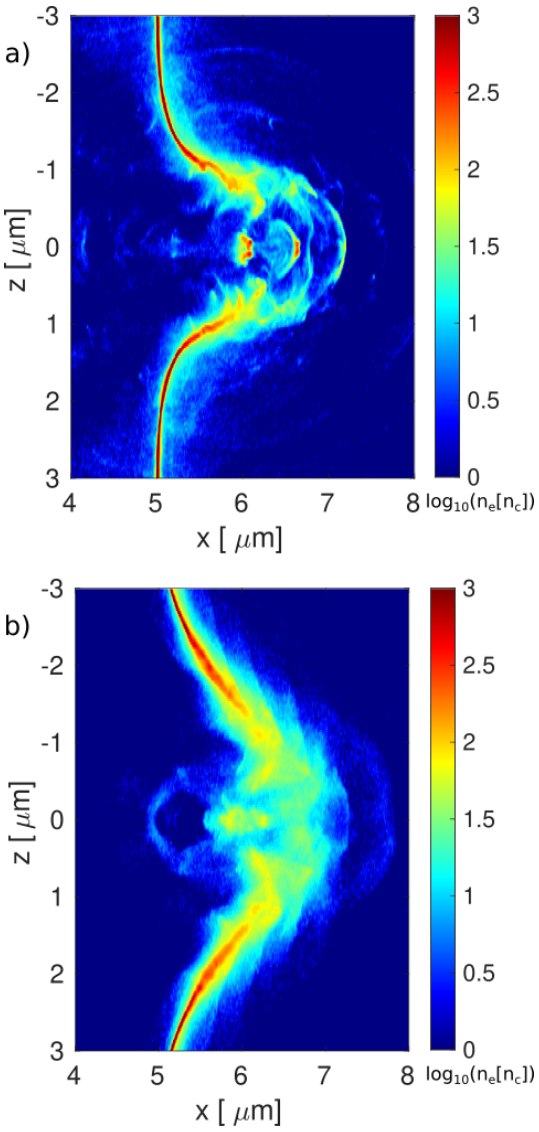

Figure 3: *Logarithm of electron density of silver target in x-z plane from 3D simulations: a) with the plasma shutter, b) without it.*

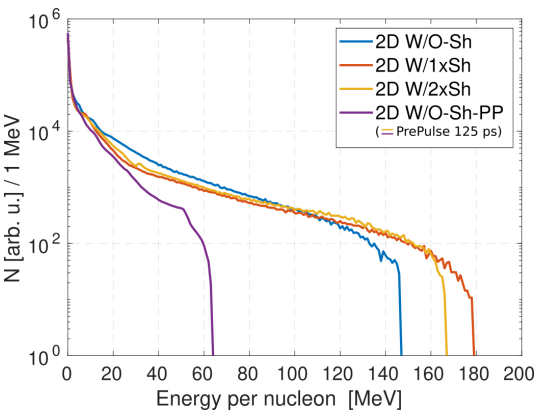

Figure 4: *Silver ion energy spectra in 2D.*

paring the two cases with prepulse included (W/O-Sh-PP and W/2xSh) results in the increase of maximal ion energy from 64 MeV/A to 167 MeV/A.

In conclusion application of the steep rising front (and increased intensity) generated by the plasma shutter in our 3D simulations resulted in increase of maximal silver ion energy by 35 %, reduce of divergence of ion beam by 20° in the dominate plane and generation of high density electron bunches . The assumed double plasma shutter scenario (taking into account a 125 ps prepulse) results in significant increase of maximal silver ion energy.

Portions of this research were carried out at ELI Beamlines, a European user facility operated by the Institute of Physics of the Academy of Sciences of the Czech Republic. Our work is supported by projects: High Field Initiative (CZ.02.1.01/0.0/0.0/15_003/0000449) and Center of Advanced Applied Sciences (CZ.02.1.01/0.0/0.0/16_019/0000778) from the European Regional Development Fund. This work was supported by the Ministry of Education, Youth and Sports of the Czech Republic through the e-INFRA CZ (ID:90140). Access to CESNET storage facilities provided by the project e-INFRA CZ under the programme Projects of Large Research, Development, and Innovations Infrastructures (LM2018140), is appreciated. The data post-processing was performed using computational resources funded from the CAAS project. The support of Grant Agency of the Czech Technical University in Prague is appreciated, grants no. SGS22/185/OHK4/3T/14 and SGS22/184/OHK4/3T/14.

References

[1] M. Matys, K. Nishihara, M. Kecova, et al., High Energy Density Physics **36**, 100844 (2020).

[2] F. Pegoraro and S.V. Bulanov, Physical Review Letters **99**, 065002 (2007).

[3] V. A. Vshivkov, N. M. Naumova, F. Pegoraro and S. V. Bulanov, Physics of Plasmas **5**, 2727 (1998).

[4] S. A. Reed, T. Matsuoka, S. Bulanov, et al., Applied Physics Letters **94**, 201117 (2009).

[5] S. Palaniyappan, B. M. Hegelich, H. C. Wu, et al., Nature Physics **8**, 763-769 (2012).

[6] W. Q. Wei, X. H. Yuan, Y. Fang, et al., Physics of Plasmas **24**, 113111 (2017).

[7] M. Matys, O. Klimo, J. Psikal and S. V. Bulanov, Europhysics conference abstracts, **42A**, P4.2031 (2018).

[8] M. Jirka, O. Klimo, Y.-J. Gu and S. Weber, Scientific Reports **10**, 8887 (2020).

[9] M. Jirka, M. Matys and O. Klimo, Physical Review Research **3**, 033175 (2021).

[10] M. Matys, S. V. Bulanov, M. Kecova, et al., Proc. SPIE **11779**, Laser Acceleration of Electrons, Protons, and Ions VI, 117790Q (2021).

[11] M. Matys, S. V. Bulanov, M. Kucharik, et al., arXiv:2205.06088 (2022).

[12] T. D. Arber, K. Bennett, C. S. Brady, et al., Plasma Physics and Controlled Fusion **57**, 113001 (2015).

[13] R. Liska, M. Kucharik, J. Limpouch, et al., Finite Volumes for Complex Applications VI Problems & Perspectives **978-3-642-20671-9**, 857-873, Springer, Berlin (2011).

[14] B. Gonzalez-Izquierdo , R. Gray , M. King, et al., Nature Physics **12** 505512 (2016).

[15] A. Levy, T. Ceccotti, P. D'Oliveira, et al., Optics Letters **32** 310-312 (2007).